



Synthesis and lithium insertion properties of ramsdellite Li_xTiO_2 anode materials



Isao Tsuyumoto*, Takumi Moriguchi

Department of Applied Chemistry, College of Bioscience and Chemistry, Kanazawa Institute of Technology, 7-1 Ohgigaoka, Nonoichi, Ishikawa 921-8501, Japan

ARTICLE INFO

Article history:

Received 3 May 2015

Received in revised form 2 June 2015

Accepted 6 June 2015

Available online 9 June 2015

Keywords:

A. Oxides

B. Sol–gel chemistry

C. Electrochemical measurements

C. X-ray diffraction

D. Electrochemical properties

ABSTRACT

Ramsdellite Li_xTiO_2 ($x=0.47$) with reduced form is successfully prepared as a single phase by heating an amorphous lithium peroxy-polytitanate in 4.8% H_2 at 1100 °C for 0–1 h. The XRD data are well refined with the space group $Pnma$ with $a=0.96076$ nm, $b=0.29514$ nm and $c=0.50276$ nm. The ramsdellite Li_xTiO_2 transforms into a rutile–ramsdellite intergrowth phase by extending the heating time to 1.25–4 h. The capacity of the ramsdellite Li_xTiO_2 in the region of 1.0–2.5 V (vs Li) is 208 mAh g^{-1} at 0.8 C rate (0.13 mA mg^{-1}), substantially larger than that of the ramsdellite $\text{Li}_2\text{Ti}_3\text{O}_7$ with oxidized form. The lithium insertion and deinsertion proceeds in two stages: a sloping region at higher potential (1.4–2.3 V) and a plateau region at lower potential (1.3–1.4 V).

©2015 Elsevier Ltd. All rights reserved.

1. Introduction

Lithium titanates have been widely investigated as anode materials for lithium ion batteries since early 1990s, because they allow safer operating conditions compared to graphite electrodes due to higher working potential which does not give rise to Li electroplating (Li^+ reduction) [1–5]. Spinel-type $\text{Li}_{4/3}\text{Ti}_5/3\text{O}_4$ shows good cycle characteristics with little capacity loss due to no noticeable lattice dimension change during lithium insertion and deinsertion processes [4] and is already in practical use in commercially available lithium ion batteries [2].

Ramsdellite $\text{Li}_2\text{Ti}_3\text{O}_7$ and Li_xTiO_2 ($0 \leq x \leq 0.57$) have also attracted much attention as anode materials for lithium ion batteries, because in the ramsdellite structure the double columns of TiO_6 octahedra form open framework with tunnels along c axis favorable for lithium insertion (Fig. 1) [2,6–8]. The ramsdellite $\text{Li}_2\text{Ti}_3\text{O}_7$ with oxidized form is colorless and shows great lithium ionic conductivity around $1.2 \times 10^{-6} \text{ S cm}^{-1}$ and negligible electronic conductivity at 25 °C [6], while the ramsdellite $\text{Li}_{0.5}\text{TiO}_2$ with reduced form is black [9,10] and shows room-temperature resistivity of 60 Ωcm [11] due to electronic conduction via mixed valence state between Ti^{3+} and Ti^{4+} . The ramsdellite $\text{Li}_2\text{Ti}_3\text{O}_7$ and Li_xTiO_2 belong to the same space group $Pbnm$, but the distribution situation of Li and Ti in the framework differs to compensate the difference in the Ti/O ratio. In the structure of Li_xTiO_2 , the

occupancy of Ti in the 4c site at the center of the TiO_6 octahedra is unity, and all Li atoms are located in the tunnels [9,10,12]. On the other hand, in the structure of $\text{Li}_2\text{Ti}_3\text{O}_7$, one-seventh of Ti in the 4c site is replaced by Li to adjust the Ti/O ratio at 3/7 [13–18], and thus the compositional formula is more properly represented by $\text{Li}_{3/7}[\text{Li}_{1/7}\text{Ti}_{6/7}]\text{O}_2$. Since this atomic replacement is considered to cause structural instability and to impair the reversibility of lithium insertion, we can expect better charge–discharge performance of the reduced-form ramsdellite Li_xTiO_2 .

While a substantial number of reports have appeared on the preparation, structure and electrochemistry of the oxidized form, $\text{Li}_2\text{Ti}_3\text{O}_7$ [6,13–24], there have been few reports on the reduced form, Li_xTiO_2 [7,8]. Soares et al. prepared delithiated Li_xTiO_2 ($0 \leq x \leq 0.57$) from a homogeneously ground mixture of Li_2CO_3 , TiO_2 and sucrose through a carbothermal synthesis route and reported that the delithiation of the ramsdellite Li_xTiO_2 was accompanied by the growth of a secondary spinel phase [8]. Homogeneous starting materials and controlled synthetic conditions were suggested to be essential for the preparation of the ramsdellite Li_xTiO_2 .

New synthetic routes of metal oxides from peroxy-metallic acid formed by reaction of metallic powder with concentrated hydrogen peroxide have been developed in our previous study [25–27]. For example, peroxy-polytitanic acid (Ti-iPA where iPA stands for isopolyacid) solution was formed by reaction of metallic titanium powder with 30–70 wt% hydrogen peroxide solution, and nanocrystalline anatase TiO_2 was prepared by heating a dry residue of the Ti-iPA solution at 300–500 °C [28–31]. The thus-prepared anatase TiO_2 showed good lithium insertion and deinsertion

* Corresponding author. Fax: +81 76 294 6713.

E-mail address: tsuyu@neptune.kanazawa-it.ac.jp (I. Tsuyumoto).

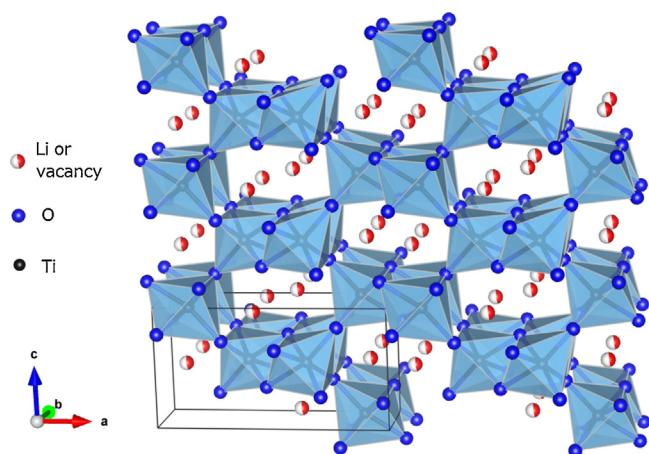


Fig. 1. Perspective view of the ramsdellite Li_xTiO_2 crystal structure projected along b axis.

performance [32]. Nanosized tetragonal BaTiO_3 was also prepared by heating a precipitate obtained by mixing Ti-iPA solution with $\text{Ba}(\text{OH})_2$ solution at 600–650 °C [33]. We considered such synthetic routes from Ti-iPA allowing uniform mixing of the constituent elements of raw materials at atomic level were appropriate for preparation of lithium titanates, because the conventional solid state reactions required repeated heating and grinding for long periods. In this study, we investigated synthetic conditions for the lithium titanates and successfully developed a new synthetic route of ramsdellite Li_xTiO_2 as a single phase from the mixture of Ti-iPA and lithium carbonate solutions. We present here its synthetic procedure, crystal structure, and lithium insertion and deinsertion properties as an anode for lithium ion batteries.

2. Experimental

2.1. Synthesis procedure

Ti-iPA was prepared according to our previously reported method [32,33]. In short, metallic titanium powder (0.17 g, 45 μm particle size, as received from Wako Pure Chemical Industries Ltd., Osaka, Japan) was dissolved in 150 mL of 30 wt% aq. H_2O_2 solution (Wako Pure Industries Ltd., Osaka, Japan) at 20 °C with stirring, and a yellow transparent Ti-iPA solution was obtained in 24 h. After filtration to remove insolubles, Li_2CO_3 (Wako Pure Industries Ltd.,

Osaka, Japan) was added to the Ti-iPA solution at a molar mixing ratio of $\text{Li}/\text{Ti} = 0.75$. The mixed solution was dried at 115 °C for 24 h in air to yield a pale yellow amorphous powder, lithium peroxo-polytitanate. The products were obtained by heating the amorphous powder at 1100 °C in a reducing atmosphere of 4.8% H_2 in Ar in a quartz tube, where the temperature was increased at 24 °C min^{-1} to 600 °C, at 11 °C min^{-1} from 600 °C to 1000 °C, and 1.7 °C min^{-1} from 1000 to 1100 °C. The final products were rapidly quenched from 1100 °C in 4.8% H_2 in order to suppress the formation of byproduct. For comparison, the product using the conventional solid state reaction of a well-ground mixture of Li_2CO_3 and rutile TiO_2 ($\text{Li}/\text{Ti} = 0.75$) under the same heating condition was also investigated.

2.2. Characterization

The Li/Ti ratios of the products were determined by inductively coupled plasma atomic emission spectroscopy (ICP-AES). Sample solutions for ICP-AES were prepared by dissolving 8.5 mg of the products into 20 mL of 36 wt% HCl aq. and diluting them with ultrapure water from Milli-Q system (Millipore, USA). The X-ray diffraction (XRD) patterns of the products were measured with a diffractometer (XD-D1, Shimadzu, Kyoto, Japan) using graphite-monochromatized $\text{Cu K}\alpha$ radiation ($\lambda = 0.15406 \text{ nm}$) at 30 kV and 30 mA. The X-ray profiles were collected between 2° and 120° of 2θ angles with a step interval of 0.02° and a count time of 1 s/step. The XRD samples were mixed with paraffin at weight ratio of 1:1 in order to avoid oxidation by air during the XRD measurement. The crystalline parameters were refined by the Rietveld method using the RIETAN-FP program [34,35], and the crystallite sizes were estimated by the Scherrer equation. The morphology was observed by a scanning electron microscope (SEM, JSM-5610, JEOL, Tokyo, Japan) with an accelerating voltage of 10 kV. Electrochemical measurements were performed using three electrode type cells assembled in an Ar-filled glove box. For a working electrode, each sample of 5.02–5.04 mg was intimately ground with acetylene black (AB) as conductive auxiliary agent, and the composite, after mixing with polytetrafluoroethylene (PTFE) as a binder, was pressed onto a copper mesh. The weight ratio of sample:AB:PTFE was 40:40:20. Li metal was used as reference and counter electrodes. The electrolyte used was a 1 M solution of LiPF_6 in ethylene carbonate (EC)/diethyl carbonate (DEC) solution (1:1 by volume, Kishida Chemical, Osaka, Japan). Cyclic voltammetric profiles were recorded at scan rates of 0.20–3.33 mV s^{-1} in the range of 0.8–3.0 V (vs Li), and charge–discharge measurements

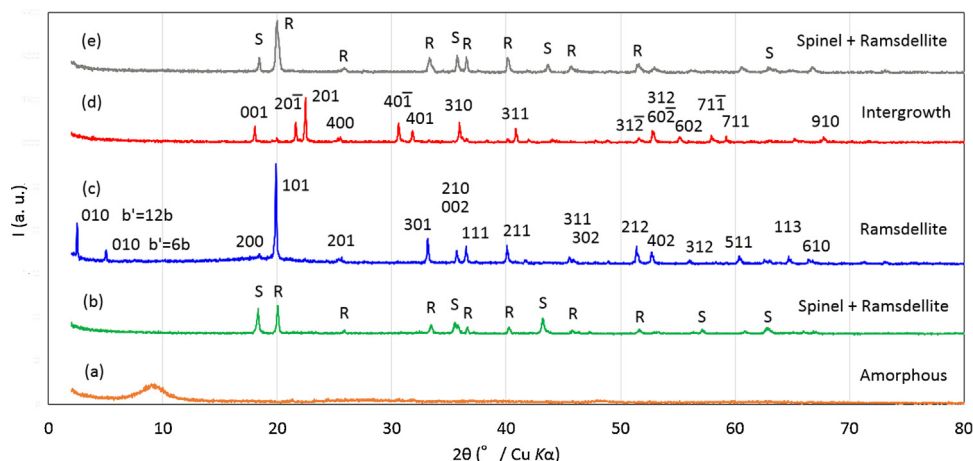


Fig. 2. XRD patterns of the products obtained by heating lithium peroxo-polytitanate in 4.8% H_2 along with that by the solid state reaction. (a) lithium peroxo-polytitanate dried at 115 °C in air, (b) heating lithium peroxo-polytitanate at 950 °C for 1 h in 4.8% H_2 , (c) heating lithium peroxo-polytitanate at 1100 °C for 1 h in 4.8% H_2 , (d) heating lithium peroxo-polytitanate at 1100 °C for 4 h in 4.8% H_2 , and (e) heating the mixture of Li_2CO_3 and TiO_2 at 1100 °C for 1 h in 4.8% H_2 .

were carried out in the galvanostatic mode at 0.653–3.26 mA (0.130–0.649 mA mg⁻¹) in the range of 0.8–3.0 V (vs Li).

3. Results and discussion

3.1. Synthesis

A black ramsdellite lithium titanate with reduced form, Li_xTiO₂, was obtained as a single phase by heating at 1100 °C for 0–1 h in a reducing atmosphere of 4.8% H₂ in Ar (Fig. 2c). At 950–1000 °C the ramsdellite Li_xTiO₂ was formed with a considerable amount of the spinel Li₄Ti₅O₁₂ (Fig. 2b), the fraction of the spinel phase was decreased with elevating the heating temperature, and the ramsdellite phase was obtained as a single phase at 1070–1100 °C. By extending the reducing time to 1.25–4 h at 1100 °C, the products transformed into a rutile–ramsdellite intergrowth phase, in which the tunnels were composed of alternating double and single columns (Fig. 2d) [36]. The Li/Ti ratios of the products reduced at 1100 °C for 0, 0.75, 1.00 and 1.25 h were 0.49, 0.47, 0.47 and 0.37, respectively, from ICP analysis. This suggests that the ramsdellite Li_xTiO₂ is stable when $x \geq 0.47$ and that it transforms to the intergrowth phase when x falls below 0.47 due to the volatilization of lithium at 1100 °C. In the present case, the transformation to the intergrowth phase seems to also enhance the volatilization of lithium because the Li/Ti ratio abruptly decreases between the heating time 1.00 and 1.25 h. It was also found that the ramsdellite Li_xTiO₂ ($x=0.47$ –0.49) with dark blue color was oxidized in air at room temperature to its oxidized form with gray color. The conventional solid state reaction between Li₂CO₃ and TiO₂ at 1100 °C for 1 h in a reducing atmosphere of 4.8% H₂ in Ar resulted in the formation of the mixture of the ramsdellite Li_xTiO₂ and the spinel Li₄Ti₅O₁₂ (Fig. 2e). This suggests that homogeneous starting materials in which constituent elements are uniformly mixed at atomic level are advantageous for preparing complex oxides in a short reaction time.

3.2. Structural characterization

The structural parameters of the single phase ramsdellite Li_xTiO₂ ($x=0.47$) obtained from the Rietveld refinement are summarized in Table 1. The crystal structure was similar to the ramsdellite Li_{0.5}TiO₂ reported by Akimoto et al. [9]. All the XRD data were well refined with the orthorhombic space group *Pnma* with $a=0.96076$ nm, $b=0.29514$ nm, and $c=0.50276$ nm. The structure has four Ti, eight O, and 1.88 Li atoms per unit cell. Distorted TiO₆ octahedra form double columns along *b* axis by sharing their edges, which give rise to open framework with tunnels running along the *b* axis. Lithium ions are located in the tunnels, in which two Li sites at the same *y* coordinate are occupied by 47% Li ions on average. Interestingly, as shown in Fig. 2c, long-range periodicity was first observed along the *b* axis. The peak at 2.50° corresponds to 010 reflection when the lattice constant of the *b* axis becomes twelve times larger than that of the original unit

Table 1

Refined crystallographic data for Li_xTiO₂ obtained by heating the amorphous lithium peroxo-polytitanate in 4.8% H₂ at 1100 °C.

Orthorhombic; Space group; <i>Pnma</i> (62) Z=4					
$a=0.9608$ nm $b=0.2951$ nm $c=0.5028$ nm Crystallite size: 69.2 nm					
Atom	Site	<i>x</i>	<i>y</i>	<i>z</i>	Occupancy
Li	4c	0.417	0.25	-0.061	0.47
Ti	4c	0.141	0.25	-0.024	1.0
O(1)	4c	0.274	0.25	0.691	1.0
O(2)	4c	-0.035	0.25	0.186	1.0

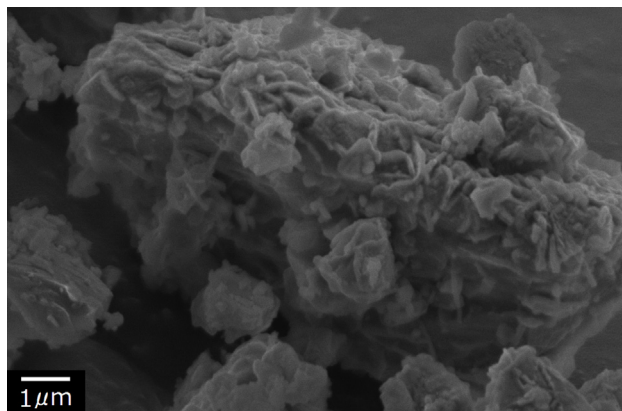


Fig. 3. SEM image of the ramsdellite Li_{0.47}TiO₂ obtained by heating lithium peroxo-polytitanate in 4.8% H₂ at 1100 °C for 1 h.

cell, i.e., $b' = 12b$, and the peak at 5.02° corresponds to 010 reflection when $b' = 6b$. This suggests that the lithium ions and their vacancies in the tunnels are arranged periodically every twelve unit cells along the *b* axis. Fig. 3 shows the morphology of the ramsdellite Li_{0.47}TiO₂. Plate-like particles with diameter ranging from submicron to micron scale were observed in the SEM image, while the crystallite size was estimated at 69.2 nm using the Scherrer equation from the XRD pattern. Secondary particles consisting of several tens nanometer scale crystallites are considered to be observed in the SEM image, and this suggests that intimate mixing with conductive auxiliary agent at several tens nanometer scale is essential for preparation of the working electrode to extract optimal performance as lithium insertion electrodes [37–39].

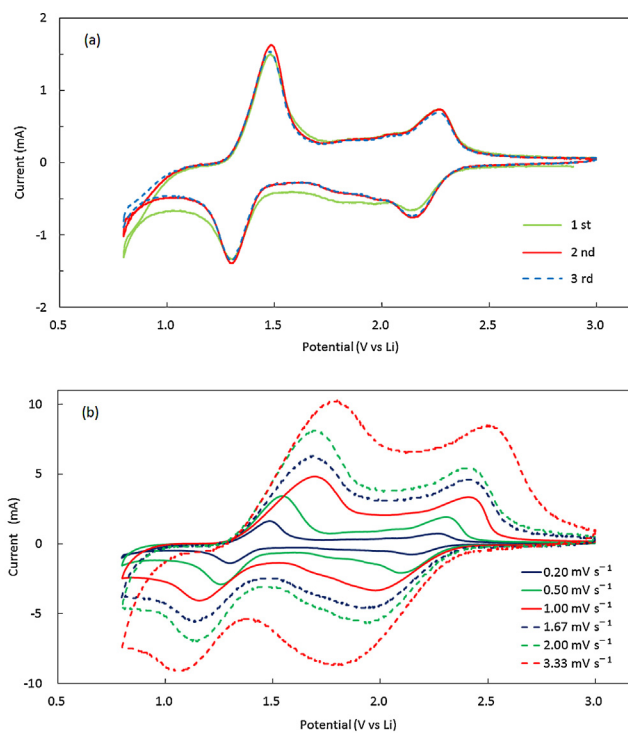


Fig. 4. (a) first three CV profiles of the ramsdellite Li_{0.47}TiO₂ at a scan rate of 0.2 mV s⁻¹, and (b) second CV profiles of the ramsdellite Li_{0.47}TiO₂ at different scan rates from 0.2 to 3.3 mV s⁻¹.

3.3. Electrochemical properties

Fig. 4a shows the CV profiles of the ramsdellite $\text{Li}_{0.47}\text{TiO}_2$ at a scan rate of 0.20 mV s^{-1} . Two large cathodic peaks at 2.15 and 1.31 V and two large anodic peaks at 1.48 and 2.26 V were observed during the reversible lithium insertion and deinsertion process in the range of 0.8–3.0 V (vs Li). This indicates that the insertion and deinsertion proceed in two stages at higher and lower potential (stages H and L after this, respectively). In reported studies, the CV profiles of the oxidized-form ramsdellite $\text{Li}_2\text{Ti}_3\text{O}_7$ showed only an extra shoulder peak on the principal 1.5 V peak, while the phases in the $\text{Li}_{1+x}\text{Ti}_{2-2x}\text{O}_4$ system ($x=0-0.1$) showed additional smaller peaks in the range of 1.5–2 V [7]. The additional peaks at higher potential seem to be peculiar to the reduced-form ramsdellite titanates. Although the possibility of the presence of several Li insertion sites was mentioned in the report, details on the two peaks have not been clarified so far.

Fig. 4b shows the CV profiles of the ramsdellite $\text{Li}_{0.47}\text{TiO}_2$ at different scan rates. The peak current values were increased with increasing the scan rate, suggesting diffusion-controlled insertion and deinsertion. The relationship between the peak current values and the scan rates are described by

$$\frac{I_p}{m} = 2.69 \times 10^5 n^{3/2} A c v^{1/2} D^{1/2}, \quad (1)$$

where I_p is the peak current, m is the mass of electrode, n is the number of transferred electrons, A is an electrode surface area per unit mass, c is the concentration of lithium in $\text{Li}_{0.47}\text{TiO}_2$, v is the scan rate, and D is the apparent diffusion coefficient that incorporates both Li diffusion in the bulk and Li transfer through the interface [40,41]. c is calculated as $0.0219 \text{ mol cm}^{-3}$ because $\text{Li}_{0.47}\text{TiO}_2$ has a bulk density of 3.88 g cm^{-3} , a molar mass of 83.2 g mol^{-1} , and a Li composition of 0.47. As for $\text{Li}_{0.47}\text{TiO}_2$, one-third of the total electrode surface area should be used as the electrode surface area A , because the diffusion occurs in the one-dimensional channels along b axis and only (0 1 0) plane is effective for diffusion. A is calculated as $7.46 \times 10^4 \text{ cm}^2 \text{ g}^{-1}$ from the mean crystallite diameter of 69.2 nm from the XRD pattern and the bulk density. The apparent diffusion coefficients, D , for the stages H and L were determined from the slope of I_p/m vs $v^{0.5}$ plot at 6.0×10^{-15} and $8.0 \times 10^{-15} \text{ cm}^2 \text{ s}^{-1}$ for anodic diffusion, and 6.3×10^{-15} and $6.3 \times 10^{-15} \text{ cm}^2 \text{ s}^{-1}$ for cathodic diffusion, respectively.

Charge–discharge curves of the reduced-form ramsdellite $\text{Li}_{0.47}\text{TiO}_2$ in the range of 0.8–3.0 V (vs Li) at 0.8 C rate (0.4 Li/1 h) are shown in Fig. 5. Two-stage processes were observed in both of the insertion and deinsertion curves: a sloping region at higher potential (1.4–2.3 V) and a plateau region at lower potential (1.3–1.4 V). The capacities were 201–208 mAh g^{-1} in the region of 1.0–2.5 V (vs Li) except for the first charge process presumably

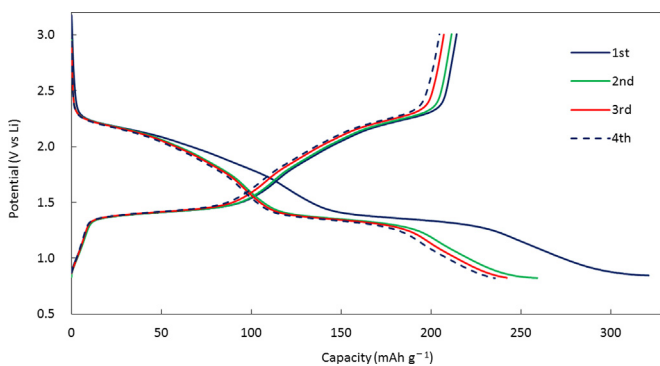


Fig. 5. Charge–discharge curves of the ramsdellite $\text{Li}_{0.47}\text{TiO}_2$ at a current density of 0.13 mA mg^{-1} (0.8 C).

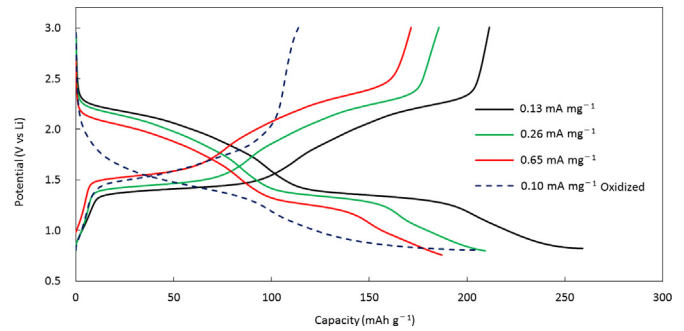


Fig. 6. The second charge–discharge curves of the reduced form–ramsdellite $\text{Li}_{0.47}\text{TiO}_2$ at different current densities of 0.13, 0.26, and 0.65 mA mg^{-1} (0.8, 1.6, and 4.0 C), along with that of the oxidized-form ramsdellite $\text{Li}_2\text{Ti}_3\text{O}_7$ at a current density of 0.10 mA mg^{-1} .

partly consumed for the formation of the SEI (solid electrolyte interface) layer, and these values are comparable to the spinel phase $\text{Li}_4\text{Ti}_5\text{O}_{12}$. The second charge–discharge curves of the reduced-form ramsdellite $\text{Li}_{0.47}\text{TiO}_2$ at rates of 0.8, 1.6, and 4.0 C are shown in Fig. 6, along with that of the oxidized-form ramsdellite $\text{Li}_2\text{Ti}_3\text{O}_7$ at a rate of 1.0 C obtained by heating in Ar at 1100°C for 0 h for comparison. With increasing the rate, the capacities of the plateau region at lower potential were decreased more rapidly than those of the sloping region at higher potential. The sloping and plateau regions correspond with the stages H and L, respectively, observed in the CV profiles, and the rate dependence of each region can be related to an accommodation mechanism for Li ions. Furthermore, the capacities of the reduced-form ramsdellite were increased with increasing the heating time from 0 to 1 h at 1100°C probably due to the improvement of crystallinity, while the intergrowth phase formed as a byproduct by heating for 1.25 h or more brought about the reduction of the capacities. This suggests that the rutile–ramsdellite intergrowth type is unfavorable for lithium insertion and deinsertion, though half of the channels are composed of the double columns. The oxidized-form ramsdellite $\text{Li}_2\text{Ti}_3\text{O}_7$ showed similar behavior to those of the conventional ramsdellite $\text{Li}_2\text{Ti}_3\text{O}_7$ reported in the earlier research, differently from those of the reduced-form ramsdellite $\text{Li}_{0.47}\text{TiO}_2$, and the capacities were about 100–120 mAh g^{-1} in the region of 1.0–3.0 V (vs Li), much smaller than those of the reduced form. The two-stage curves were peculiar to the reduced form. The plateau regions can be explained by assuming a two-phase equilibrium in the reduced-form ramsdellite $\text{Li}_{0.47}\text{TiO}_2$. When there are two phases, e.g., Li_aTiO_2 – Li_bTiO_2 and Li_bTiO_2 – Li_cTiO_2 ($a < b < c$), and an equilibrium is established between $\text{Li}_{x_1}\text{TiO}_2$ in the former phase and $\text{Li}_{x_2}\text{TiO}_2$ in the latter phase at certain values of x_1 and x_2 ($a < x_1 < b$, $b < x_2 < c$), the lithium content change in the range from x_1 to x_2 occurs through phase transitions between $\text{Li}_{x_1}\text{TiO}_2$ and $\text{Li}_{x_2}\text{TiO}_2$. In other words, the lithium insertion and deinsertion bring about the change in the fraction of each phase, not in the lithium content of each phase. In this case, the electrode potential remains constant in spite of the lithium content change, because $\text{Li}_{x_1}\text{TiO}_2$ and $\text{Li}_{x_2}\text{TiO}_2$ have the same chemical potential. Similar plateau behavior has been reported for the ramsdellite TiO_2 , and a comparable mechanism involving two two-phase equilibria has been proposed [7]. Considering the experimental fact that such plateau behavior was not observed for the oxidized-form ramsdellite $\text{Li}_2\text{Ti}_3\text{O}_7$, the two phase equilibrium is expected to be established when Ti is deeply reduced and close to the trivalent state. It is highly desirable to extend the plateau region capacity to apply it to the lithium ion batteries, and we expect that this will be possible by investigating precisely phase diagrams of the reduced-form ramsdellite and designing an oxide with optimum composition and valence.

4. Conclusions

We developed a new synthesis method of the reduced-form ramsdellite Li_xTiO_2 as a single phase using an amorphous lithium peroxy-polytitanate. We found that the lithium insertion and deinsertion performance as anode materials of the lithium ion batteries was much higher than the oxidized-form ramsdellite $\text{Li}_2\text{Ti}_3\text{O}_7$ and comparable to the spinel $\text{Li}_4\text{Ti}_5\text{O}_{12}$. The capacity was 208 mAh g^{-1} at 0.8 C in the region of 1.0–2.5 V (vs Li). The reduced-form Li_xTiO_2 showed peculiar two-stage processes in both of the insertion and deinsertion curves: a sloping region at higher potential and a plateau region at lower potential. It is highly desirable to extend the plateau region at lower potential for practical use, and the plateau region is presumably due to a two-phase equilibrium. Our future challenge is to elucidate the two phases in equilibrium and to prepare a ramsdellite $\text{Li}_x\text{Ti}_y\text{O}_{2-z}$ with an optimum composition.

Acknowledgements

The authors are sincerely grateful to Prof. Yujiro Watanabe of Kanazawa Institute of Technology for assistance in ICP analysis. This work was supported by a Grant-in-Aid for Scientific Research (C), No. 25410244, from the Japan Society for the Promotion of Science (JSPS).

References

- [1] Z. Yang, D. Choi, S. Kerisit, K.M. Rosso, D. Wang, J. Zhang, G. Graff, J. Liu, Nanostructures and lithium electrochemical reactivity of lithium titanates and titanium oxides: a review, *J. Power Sources* 192 (2009) 588–598.
- [2] G. Zhu, Y. Wang, Y. Xia, Ti-based compounds as anode materials for Li-ion batteries, *Energy Environ. Sci.* 5 (2012) 6652–6667.
- [3] K.M. Colbow, J.R. Dahn, R.R. Haering, Structure and electrochemistry of the spinel oxides LiTi_2O_4 and $\text{Li}_{4/3}\text{Ti}_{5/3}\text{O}_4$, *J. Power Sources* 26 (1989) 397–402.
- [4] T. Ohzuku, A. Ueda, N. Yamamoto, Zero-strain insertion material of $\text{Li}[\text{Li}_{1/3}\text{Ti}_{5/3}]_2\text{O}_4$ for rechargeable lithium cells, *J. Electrochem. Soc.* 142 (5) (1995) 1431–1435.
- [5] L. Kavan, J. Procházka, T.M. Spitzer, M. Kalbác, M. Zúkalová, T. Drezen, M. Grätzel, Li insertion into $\text{Li}_4\text{Ti}_5\text{O}_{12}$ (spinel), *J. Electrochem. Soc.* 150 (7) (2003) A1000–A1007.
- [6] J.B. Boyce, J.C. Mikkelsen Jr., Anisotropic conductivity in a channel structured superionic conductor: $\text{Li}_2\text{Ti}_3\text{O}_7$, *Solid State Commun.* 31 (1979) 741–745.
- [7] R.K.B. Gover, J.R. Tolchard, H. Tukamoto, T. Murai, J.T.S. Irvine, Investigation of ramsdellite titanates as possible new negative electrode materials for Li batteries, *J. Electrochem. Soc.* 146 (1999) 4348–4353.
- [8] A. Soares, B. Fraise, F. Morato, C.M. Ionica-Bousquet, L. Monconduit, On the synthesis conditions for tailoring lithium composition in ramsdellite phases: application for Li-ion batteries, *J. Power Sources* 208 (2012) 440–446.
- [9] J. Akimoto, Y. Gotoh, M. Sohma, K. Kawaguchi, Y. Oosawa, Synthesis and crystal structure of ramsdellite-type $\text{Li}_{0.5}\text{TiO}_2$, *J. Solid State Chem.* 110 (1994) 150–155.
- [10] J. Akimoto, Y. Gotoh, Y. Oosawa, N. Nonose, T. Kumagai, K. Aoki, Topotactic oxidation of ramsdellite-type $\text{Li}_{0.5}\text{TiO}_2$, a new polymorph of titanium dioxide: $\text{TiO}_2(\text{R})$, *J. Solid State Chem.* 113 (1994) 27–36.
- [11] D.C. Johnston, Superconducting and normal state properties of $\text{Li}_{1+x}\text{Ti}_{2-x}\text{O}_4$ spinel compounds. I. preparation, crystallography, superconducting properties, electrical resistivity, dielectric behavior, and magnetic susceptibility, *J. Low Temp. Phys.* 25 (1976) 145–175.
- [12] R.K.B. Gover, J.T.S. Irvine, A.A. Finch, Transformation of LiTi_2O_4 from spinel to ramsdellite on heating, *J. Solid State Chem.* 132 (1997) 382–388.
- [13] B. Morosin, J.C. Mikkelsen Jr., Crystal structure of the Li^+ ion conductor dilithium trititanate, $\text{Li}_2\text{Ti}_3\text{O}_7$, *Acta Cryst. B* 5 (1979) 798–800.
- [14] I. Abrahams, P.G. Bruce, W.I.F. David, A.R. West, Refinement of the lithium distribution in $\text{Li}_2\text{Ti}_3\text{O}_7$ using high-resolution powder neutron diffraction, *J. Solid State Chem.* 78 (1989) 170–177.
- [15] M.E. Arroyo y de Dompablo, E. Morán, A. Várez, F. García-Alvarado, Electrochemical lithium intercalation in $\text{Li}_2\text{Ti}_3\text{O}_7$ -ramsdellite structure, *Mater. Res. Bull.* 32 (1997) 993–1001.
- [16] M.E. Arroyo y de Dompablo, A. Várez, F. García-Alvarado, Structural study of electrochemically obtained $\text{Li}_{2+x}\text{Ti}_3\text{O}_7$, *J. Solid State Chem.* 153 (2000) 132–139.
- [17] W. Cho, T. Kashiwagi, W. Ra, M. Nakayama, M. Wakihara, Y. Kobayashi, H. Miyashiro, Relationship between electrochemical behavior and Li/vacancy arrangement in ramsdellite type $\text{Li}_{2+x}\text{Ti}_3\text{O}_7$, *Electrochim. Acta* 54 (2009) 1842–1850.
- [18] C. Villevieille, M. Van Thournout, J. Scoyer, C. Tessier, J. Olivier-Fourcade, J.-C. Jumas, L. Monconduit, Carbon modified $\text{Li}_2\text{Ti}_3\text{O}_7$ ramsdellite electrode for Li-ion batteries, *Electrochim. Acta* 55 (2010) 7080–7084.
- [19] C.J. Chen, M. Greenblatt, Lithium insertion into $\text{Li}_2\text{Ti}_3\text{O}_7$, *Mater. Res. Bull.* 20 (1985) 1347–1352.
- [20] S. Garnier, C. Bohnke, O. Bohnke, J.L. Fourquet, Electrochemical intercalation of lithium into the ramsdellite-type structure of $\text{Li}_2\text{Ti}_3\text{O}_7$, *Solid State Ionics* 83 (1996) 323–332.
- [21] F. García-Alvarado, M.E. Arroyo y de Dompablo, E. Morán, M.T. Gutiérrez, A. Kuhn, A. Várez, New electrode materials for lithium rechargeable batteries, *J. Power Sources* 81–82 (1999) 85–89.
- [22] A. Kajiyama, K. Takada, K. Arihara, T. Inada, H. Sasaki, S. Kondo, M. Watanabe, Synthesis and electrochemical properties of lithium chromium titanium oxide with ramsdellite structure, *J. Electrochem. Soc.* 150 (2003) A157–A160.
- [23] L. Aldon, M. Van Thournout, P. Strobel, O. Isnard, J. Olivier-Fourcade, J.-C. Jumas, Neutron diffraction and Mössbauer studies of iron substituted $\text{Li}_2\text{Ti}_3\text{O}_7$ of ramsdellite-type as negative electrode for Li-ion accumulator, *Solid State Ionics* 177 (2006) 1185–1191.
- [24] T. Ogihara, T. Kodera, Synthesis of $\text{Li}_2\text{Ti}_3\text{O}_7$ anode materials by ultrasonic spray pyrolysis and their electrochemical properties, *Materials* 6 (2013) 2285–2294.
- [25] I. Tsuyumoto, T. Kudo, Humidity sensor using potassium hexagonal tungsten bronze synthesized from peroxy-polytungstic acid and its resistivity change mechanism, *Mater. Res. Bull.* 31 (1996) 17–28.
- [26] I. Tsuyumoto, T. Kudo, Humidity sensor using potassium hexagonal tungsten bronze synthesized from peroxy-polytungstic acid, *Sens. Actuators B* 30 (1996) 95–99.
- [27] I. Tsuyumoto, A. Kishimoto, T. Kudo, Hexagonal tungsten bronze synthesized from potassium peroxy-polytungstate and its electrical properties, *Solid State Ionics* 59 (1993) 211–216.
- [28] Y. Yagi, M. Hibino, T. Kudo, Evaluation of titanium dioxide (anatase) from oxalato-polytitanate as an active material for rechargeable lithium batteries, *J. Electrochem. Soc.* 144 (1997) 4208–4212.
- [29] T. Kudo, Y. Sasaki, M. Hashimoto, K. Matsumoto, Oxalato complexes directly formed by the reaction of interstitial with hydrogen peroxide, *Inorg. Chim. Acta* 145 (1988) 205–209.
- [30] T. Kudo, H. Okamoto, K. Matsumoto, Y. Sasaki, Peroxopolytungstic acids synthesized by direct reaction of tungsten or tungsten carbide with hydrogen peroxide, *Inorg. Chim. Acta* 111 (1986) L27–L28.
- [31] T. Kudo, A new heteropolyacid with carbon as a heteroatom in a Keggin-like structure, *Nature* 312 (1984) 537–538.
- [32] I. Tsuyumoto, K. Kobayashi, Lithium ion insertion properties of nanocrystalline anatase titanium oxides prepared from peroxy-polytitanic acid, *Solid State Ionics* 255 (2013) 60–64.
- [33] I. Tsuyumoto, M. Kobayashi, T. Are, N. Yamazaki, Nano-sized tetragonal BaTiO_3 powders synthesized by a new peroxy-precursor decomposition method, *Chem. Mater.* 22 (9) (2010) 3015–3020.
- [34] F. Izumi, K. Momma, Three-dimensional visualization in powder diffraction, *Solid State Phenom.* 130 (2007) 15–20.
- [35] K. Momma, F. Izumi, VESTA 3 for three-dimensional visualization of crystal, volumetric and morphology data, *J. Appl. Crystallogr.* 44 (2011) 1272–1276.
- [36] J. Akimoto, Y. Gotoh, Y. Oosawa, Synthesis and crystal structure of $\text{Li}_x\text{Ti}_3\text{O}_6$ ($x=0.74$): an intergrowth phase of rutile and ramsdellite structure, *J. Solid State Chem.* 129 (1) (1997) 7–11.
- [37] Y. Wang, Z.-S. Feng, C. Zhang, L. Yu, J.-J. Chen, J. Hua, X.-Z. Liua, Defect effects on the physical and electrochemical properties of nanoscale $\text{LiFe}_{0.92}\text{PO}_4$ and $\text{LiFe}_{0.92}\text{PO}_4/\text{C}$ /graphene composites, *Nanoscale* 5 (9) (2013) 3704–3712.
- [38] Y. Wang, Z.-S. Feng, J.-J. Chen, C. Zhang, Synthesis and electrochemical performance of LiFePO_4 /graphene composites by solid-state reaction, *Mater. Lett.* 71 (2012) 54–56.
- [39] I. Tsuyumoto, Y. Nakakura, S. Yamaki, Nano-sized layered LiVO_2 prepared from peroxy-polyvanadic acid and its electrochemical properties, *J. Am. Ceram. Soc.* 97 (11) (2014) 3374–3377.
- [40] D.Y.W. Yu, C. Fietzek, W. Weydanz, K. Donoue, T. Inoue, H. Kurokawa, S. Fujitani, Study of LiFePO_4 by cyclic voltammetry, *J. Electrochem. Soc.* 154 (4) (2007) A253–A257.
- [41] S. Stewart, P. Albertus, V. Srinivasan, I. Plitz, N. Pereira, G. Amatucci, J. Newman, Optimizing the performance of lithium titanate spinel paired with activated carbon or iron phosphate, *J. Electrochem. Soc.* 155 (3) (2008) A253–A261.